Combining systems and synthetic biology for *in vivo* enzymology

Sara Castaño-Cerezo[1], Alexandre Chamas[2,†], Hanna Kulyk[1,3], Christian Treitz[4], Floriant Bellvert[1,3], Andreas Tholey[4], Virginie Galéote[2], Carole Camarasa[2], Stéphanie Heux[1], Luis F. Garcia-Alles[1], Pierre Millard[1,3,*] and Gilles Truan[1,*]

[1]TBI, Université de Toulouse, CNRS, INRAE, INSA, Toulouse, France

[2]SPO, Université Montpellier, INRAE, Institut Agro Montpellier, Montpellier, France

[3]MetaboHUB-MetaToul, National Infrastructure of Metabolomics and Fluxomics, Toulouse, France

[4]Systematic Proteome Research and Bioanalytics, Institute for Experimental Medicine, Christian-Albrechts-Universität zu Kiel, Kiel, Germany

[†]current address: Department of Microbial Pathogenicity Mechanisms, Leibniz Institute for Natural Product Research and Infection Biology (HKI), Jena, Germany; Cluster of Excellence Balance of the Microverse, Friedrich Schiller University Jena, Jena, Germany

*to whom correspondence should be addressed: truan@insa-toulouse.fr ; millard@insa-toulouse.fr

Abstract

Enzymatic parameters are classically determined *in vitro*, under reaction conditions that are far from those encountered in cells, casting doubt on their physiological relevance. In this study, we developed a generic approach combining tools from synthetic and systems biology to measure enzymatic parameters *in vivo*. In the context of a synthetic pathway aiming to produce phytoene and lycopene in *Saccharomyces cerevisiae*, we focused on four membrane-associated enzymes, a phytoene synthase and three phytoene desaturases, which are difficult to study *in vitro*. We designed, built, and analyzed a collection of yeast strains mimicking substantial variations in substrate concentration (> 200-fold change) by strategically manipulating the copy number and expression strength of the gene encoding geranyl-geranyl pyrophosphate (GGPP) synthase. We successfully determined *in vivo*-equivalent Michaelis-Menten parameters (K_M, V_{max} and k_{cat}) for GGPP-converting phytoene synthase from absolute metabolite concentrations, protein concentrations, and flux data, highlighting differences between *in vivo* and *in vitro* parameters. Then, leveraging the versatility of the same set of strains to cover a wide range of phytoene concentrations, we successfully extracted enzymatic parameters for two of the three phytoene desaturases. Our approach demonstrates the feasibility of assessing enzymatic parameters along a pathway of interest directly *in vivo*, providing a novel perspective on the kinetic characteristics of enzymes in real cellular conditions.

Introduction

Enzymes catalyze most of the chemical reactions in living systems. A comprehensive interpretation of enzymatic parameters is therefore of paramount importance to grasp the complexity of cellular metabolism. The vast amount of data collected for thousands of enzymes has contributed to significant progress in our understanding of the remarkable chemical capabilities of biocatalysts and of their roles in cellular reactions.

Enzymatic reactions are traditionally analyzed *in vitro*, under dilute conditions, using pure or semi-pure protein samples in buffer solution. In contrast, the cellular medium is most accurately viewed as a heterogeneous, dense, crowded gel, containing various types of macromolecules and cellular lipidic organelles, with potential partitioning effects and variations in substrate and/or product diffusion coefficients (1). The parameters determined in classical enzymology experiments may therefore not be representative of *in vivo* reaction rates and equilibrium constants (2, 3). While some progress has been made in implementing and understanding viscosity and crowding effects in *in vitro* enzymatic assays, these conditions do not mimic the intrinsic complexity of the cellular environment (2).

In vivo enzymology seems to be the obvious approach to measure enzymatic parameters inside cells. Early attempts were made using the enzyme photolyase, for which both *in vitro* and *in vivo* parameters were determined (4, 5). Meanwhile, the *in vivo* V_{max} values of ten central carbon metabolism enzymes determined in the early 90s revealed significant differences between *in vivo* and *in vitro* assays for heteromeric protein complexes (6). The past ten years have seen growing interest from systems biology in determining the *in vivo* k_{cat} of native enzymes in model organisms. The *in vivo* apparent k_{cat} of *E. coli* enzymes have been determined independently by two research groups, leveraging advances in absolute protein quantification and high throughput metabolomics (7, 8). These values were obtained by dividing the flux of enzymatic reactions by the absolute abundance of the corresponding enzymes. Both studies found correlations between *in vivo* and *in vitro* data (with correlation coefficients around 0.6), suggesting that this method could serve as an alternative to *in vitro* assays. While this systems biology approach has provided valuable information, it cannot be employed to determine apparent K_Ms *in vivo*. Zotter et al. measured the activity and affinity of TEM1-β lactamase in mammalian cells *in vivo* with confocal microscopy, using a fluorescently tagged enzyme and a fluorescent substrate and product (9). They observed that the catalytic efficiency (k_{cat}/K_M) of this enzyme differs *in vitro* and *in vivo* due to substrate attenuation, indicating that *in vitro* data are not always indicative of *in vivo* function. Zotter et al. is probably the most comprehensive *in vivo* enzymology study to date, but this approach cannot be generalized because of a lack of universally appropriate fluorescent substrates/products for all enzymes. In a recent investigation of the *in vivo* kinetic parameters of thymidylate kinase (TmK), an interesting finding was the difference in TmK's activity pattern when the substrate (thymidine monophosphate, TMP) was supplied in the media versus provided by internal metabolism, with Michaelis-Menten kinetics in the former and Hill-like kinetics in the latter. The authors hypothesized that the limited diffusion of TMP might be due to its confinement in a putative metabolon in *E. coli* (10).

In vivo enzymology is a particularly attractive prospect for membrane and multimeric proteins (6), which are tedious to purify and for which activity assays are difficult to optimize, mostly because artificial membranes are required (11–15). In the industrially important carotenoid pathway for example, despite the expression of numerous carotene biosynthesis enzymes, our understanding of their enzymatic behavior remains limited because many are membrane-associated proteins. While

kinetic parameters for some phytoene synthases, sourced from plants or bacteria, have been established *in vitro*, many enzymatic assays require the co-expression of geranylgeranyl pyrophosphate (GGPP) synthase to attain activity, possibly because of the amphiphilic nature of the substrate or the requirement of membranes (12, 15). Another example of the difficulty of *in vitro* assays is phytoene desaturase, for which discernible enzyme activity has only been achieved in engineered environments (e.g. liposomes) with cell-purified substrate (14, 16–18).

This study combines synthetic and systems biology tools to develop an original *in vivo* enzymology approach. Synthetic biology offers a remarkable set of genetic engineering tools to precisely modulate the activity of enzymes in synthetic pathways, enabling *in vivo* control of substrate concentrations for the studied enzymatic reactions. In turn, systems biology can provide quantitative data on these reactions (fluxes and enzyme, substrate and product concentrations) and computational tools to model their behavior. We applied this approach to investigate a synthetic carotenoid production pathway in *Saccharomyces cerevisiae*, with industrial applications ranging from foods to pharmaceuticals.

Results

General principle of the proposed *in vivo* enzymology method

Enzymes are usually characterized in terms of their affinity (K_M) and activity (maximal reaction rate V_{max} and turnover number k_{cat}) (Fig 1). These parameters are typically determined *in vitro* by varying the substrate concentration across a relatively broad range (about two orders of magnitude) and measuring the reaction rate for each substrate concentration (19). Different mathematical formulas, such as the Michaelis-Menten equation, have been derived to estimate enzymatic parameters from these data. We propose a novel approach wherein the substrate concentration is varied directly within cells (Fig 1), by modulating the concentration of the enzyme producing the substrate of the studied reaction. Levels of the substrate-producing enzyme are varied using different combinations of promoter strengths and gene copy numbers, and translate into a wide range of substrate concentrations (2-3 orders of magnitude, as detailed in the following sections). In our experimental setup, each substrate concentration is achieved using a specifically engineered yeast strain. In each of these strains, the gene encoding the enzyme of interest is expressed at a given level, mirroring the conditions of *in vitro* experiments. Engineered strains are then grown under steady-state conditions (i.e., exponential growth), where reaction fluxes and metabolite concentrations remain constant (20). This stability allows for the accurate measurement of product formation fluxes (equivalent to reaction rates), intracellular substrate concentrations, and enzyme concentrations. The data obtained can then be combined to calculate apparent *in vivo* kinetics parameters, denoted $K_{1/2}^{\mathrm{cell}}$, $\mathrm{V}_{\mathrm{max}}^{\mathrm{cell}}$ and $k_{\mathrm{cat}}^{\mathrm{cell}}$ in analogy with the classical K_M, V_{max} and k_{cat} parameters (Fig 1).

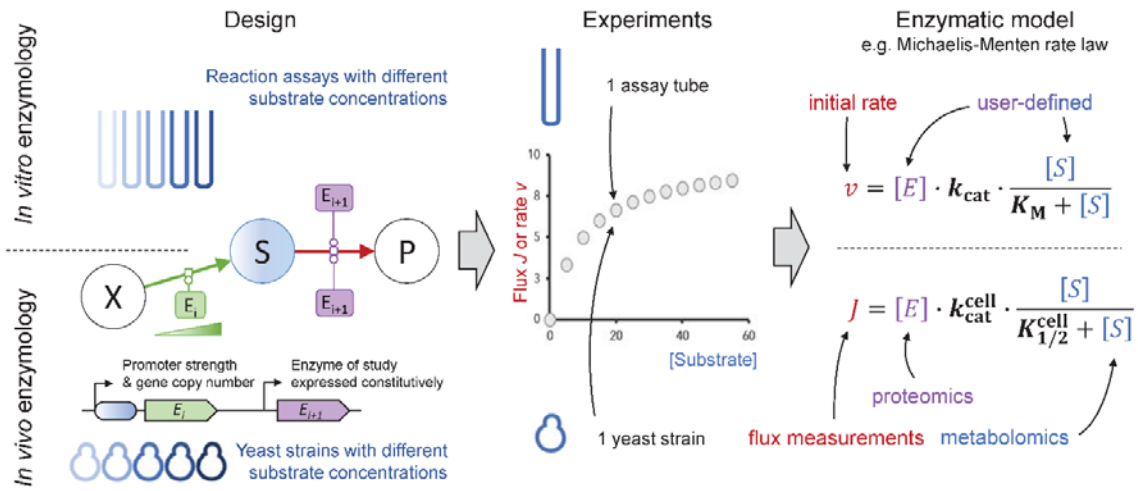

Figure 1. General principle of the proposed strategy for *in vivo* enzymology and comparison between *in vitro* and *in vivo* enzymology approaches.

Construction of yeast strains to investigate a synthetic carotenoid production pathway

We evaluated our strategy by investigating a synthetic carotenoid pathway in yeast (*S. cerevisiae*), an industrially important chassis in biotechnology, which includes two membrane-interacting enzymes that are challenging to investigate *in vitro* (12, 16, 17, 21): phytoene synthase (CrtB) and phytoene desaturase (CrtI). Phytoene synthase, the first enzyme in the carotenoid pathway and considered the bottleneck of carotenoid biosynthesis in plants (21), condenses two molecules of geranylgeranyl pyrophosphate (GGPP) head-to-head to form phytoene. Phytoene synthases have proved difficult to express in soluble and active forms in microorganisms (12, 15, 21). *In vitro* rates and affinity constants have been determined for both plant and bacterial phytoene synthases but these parameters may have been altered by the conditions of the *in vitro* assays—adding detergents for the bacterial enzyme and co-expressing a GGPP synthase or using semi-crude extracts for the plant enzyme (12, 15, 21–24). Following this enzymatic step, three insaturations are introduced in phytoene to produce lycopene. In non-photosynthetic bacteria and fungi, three reaction steps are catalyzed by a single enzyme (CrtI in bacteria and CarB in fungi) (25), whereas in plants and cyanobacteria, four different enzymes are involved in the conversion of phytoene to lycopene (26). Given that these desaturation steps are a major bottleneck in microbial carotenoid biosynthesis, determining *in vivo* enzymatic constants is an industrially relevant challenge (10, 22, 23).

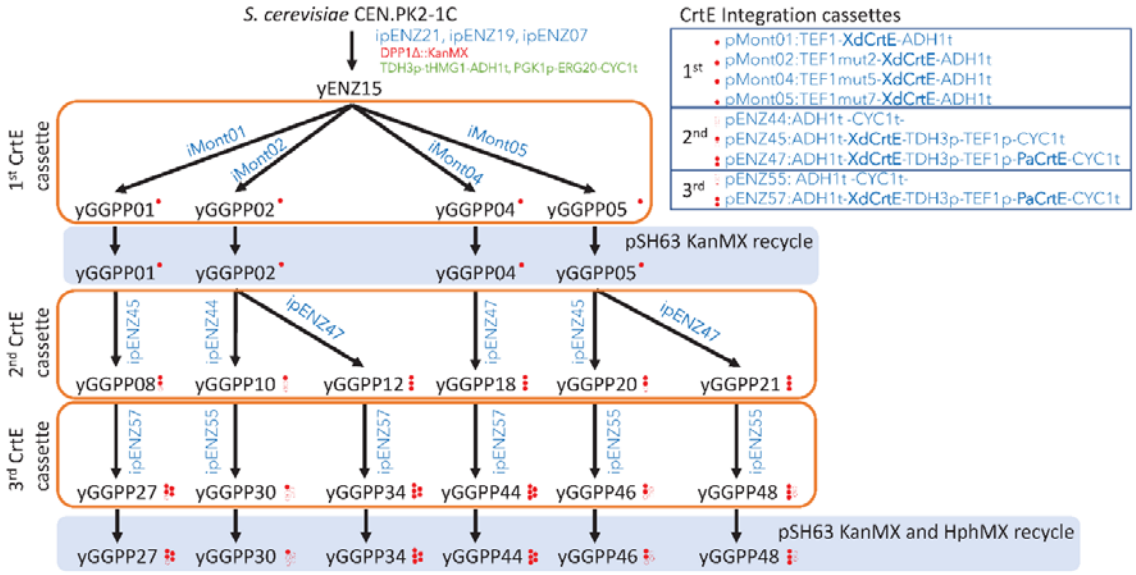

Figure 2. **Scheme of the construction of yeast strains with different GGPP concentration.** Red filled dots represent a copy of GGPP synthase, and empty dots represent an empty integration cassette.

To analyze these enzymes, we assembled a set of strains covering a broad range of substrate concentrations (Fig 2 and Table EV1). To create the collection of strains with different intracellular levels of GGPP, the substrate of phytoene synthase, we first increased GGPP production by modifying the native terpene pathway: strong constitutional expression of *ERG20* and of the truncated form of *HMG1* and deletion of the main phosphatase gene involved in GGPP and FPP pyrophosphate group removal (*DPP1*), yielding the strain yENZ15 (29, 30). Three different integration cassettes containing different microbial GGPP synthases (CrtE) expressed under different constitutive promoters were integrated into the yENZ15 genome, yielding a series of strains designed to produce a wide range of GGPP concentrations (Fig 2).

We then verified that the intracellular GGPP concentration was indeed modulated *in vivo*, as done previously (24, 32–34). GGPP concentration varied by a factor of 38 in these strains (Fig 3B), and the strains all had similar growth rates (0.40±0.03 h^{-1}) (Fig 3B) indicating that there was no change in cell physiology. As detailed below, we used this set of strains as a base to study a phytoene synthase (https://www.uniprot.org/uniprotkb/P21683/entry, EC 2.5.1.32) and three different lycopene-forming phytoene desaturases (EC 1.3.99.31).

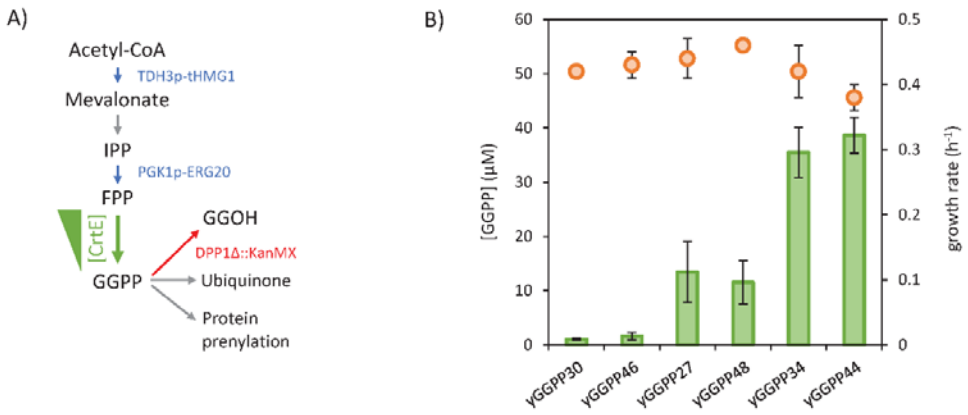

Figure 3. Construction of the set of yeast strains with different intracellular GGPP concentrations.

A Genomic modification scheme for the yENZ15 strain and intracellular fates of GGPP in *S. cerevisiae*. Overexpressed enzymes are shown in blue, enzyme deletion is shown in red, and enzyme modulation is shown in green.

B GGPP concentration (green bars) and specific growth rate of *S. cerevisiae* strains (orange dots). Mean values ± standard deviations (error bars) were estimated from three independent biological replicates.

In vivo enzymatic parameters of phytoene synthase from *Pantoea ananas*

In a classical enzymatic reaction setup, enzyme concentrations must be carefully controlled to establish an informative set of reaction rate vs substrate concentration data points. To evaluate the impact of enzyme concentration on the collected kinetic profiles, we developed a kinetic model and performed simulations for three different enzyme concentrations (low, medium and high) under a broad range of substrate-producing flux. The relationships between the steady-state substrate concentration and the flux are shown in Fig 4. Simulation results suggest that excessively high enzyme concentrations would hinder substrate saturation, rendering parameter estimation impossible. In contrast, an extremely low enzyme concentration would lead to a low production flux, making precise measurements difficult and reducing the chance of obtaining accurate enzyme parameters. Therefore, we decided to perform our saturation experiments using three enzyme concentrations by expressing *Pantoea ananas crtB* (PaCrtB) under the control of three different constitutive promoters (low expression: TEF1mut2p, medium expression: PGI1p and high expression: PDC1p).

Consistent with simulation results (Fig 4B), the GGPP concentration progressively decreased as PaCrtB activity increased (Fig 4C). Therefore, the GGPP concentration was very low at high PaCrtB level (PDC1p), and enzyme saturation was not reached. In contrast, the phytoene flux increased as PaCrtB expression increased. The phytoene concentration was too low for accurate quantification of the phytoene flux at low levels of PaCrtB (TEF1mut2p). However, accurate measurements of GGPP concentration and phytoene flux could be made at medium PaCrtB levels (PGIp). Based on these results, we used strains with medium PaCrtB levels for further investigations. A 167-fold variation in GGPP concentration (from 0.12 to 20.78 µM) was observed in these strains. Partial saturation was achieved, leading to a nonlinear relationship between the phytoene flux and the GGPP concentration, as observed in classical *in vitro* experiments. We assumed and verified, by western blot and mass spectrometry-based proteomics, that PaCrtB levels were identical in all strains (Fig EV1

189 and Table EV2), indicating that PaCrtB activity (V_{max}^{cell}) was also similar in all strains. Precise estimates
190 of V_{max}^{cell} (849±71 µM/h, rsd = 13 %) and $K_{1/2}^{cell}$ (19±3 µM, rsd = 14 %) were obtained by fitting these
191 data using an irreversible Michaelis-Menten model (consistent with previous reports (21) and with
192 the very negative ΔG^0 value of this reaction) (Table EV3). As expected from the simulations,
193 parameters could not be determined from the two other datasets (Table EV3). The affinity of PaCrtB
194 for GGPP estimated from our *in vivo* data is lower than measured *in vitro* (41 µM) (21), highlighting
195 the necessity of measuring enzyme parameters directly within the intracellular environment.
196 Meanwhile, the k_{cat}^{cell} of 6±1 s^{-1}, obtained from absolute quantitative proteomics measurements of
197 the enzyme concentration (42 nM) in strains expressing PaCrtB under the control of PGI1p, is
198 comparable to the one obtained *in vitro* for CrtB in *Pantoea agglomerans* (14 s^{-1}, Table EV4) (15).

199 The theoretical maximum phytoene production flux in these strains is therefore 849±71 µM/h. The
200 bottleneck for carotenoid biosynthesis in plants is phytoene synthase, whose activity is regulated by
201 a combination of transcriptional, post-transcriptional, and post-translational mechanisms to adjust
202 carotenoid production (35). In our synthetic system however, our results suggest that GGPP
203 biosynthesis is the limiting step since five copies of the GGPP synthase gene are required to achieve
204 just 51 % of the maximum phytoene production flux, due to the lack of phytoene synthase
205 saturation.

206

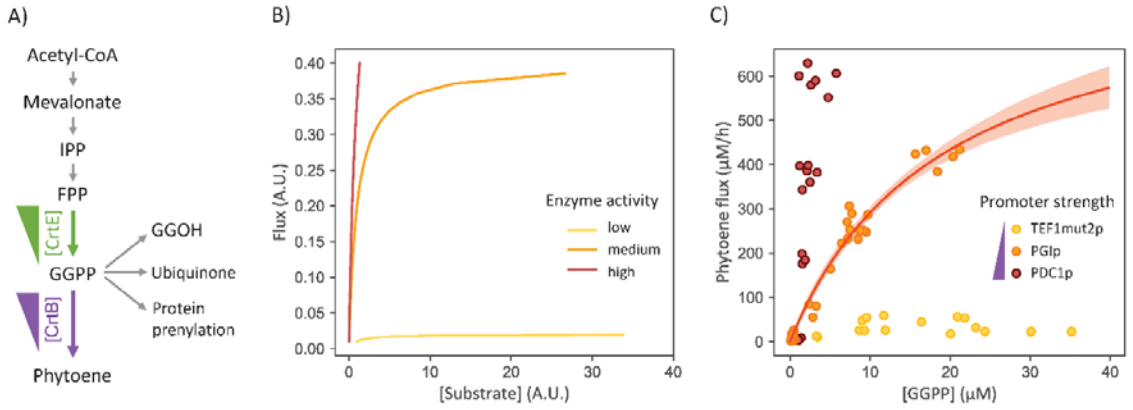

207

208

209 **Figure 4. *In vivo* characterization of phytoene synthase from *Pantoea ananas*.**

210 A Scheme for the biosynthesis of phytoene by CrtB.

211 B Steady-state flux and substrate concentration simulated for three different CrtB activities (low, medium and
212 high) under a broad range of GGPP-producing flux.

213 C *In vivo* characterization of CrtB in *S. cerevisiae*: phytoene production as a function of GGPP concentration in
214 strains with low (TEF1mut2p), medium (PGIp) and high (PDC1p) level of CrtB. Each data point represents an
215 independent biological replicate. For PGIp strains, red line represents the best fit of a Michaelis-Menten rate
216 law, and shaded area corresponds to 95 % confidence interval on the fit.

217

218 **Straightforward extension to analyze downstream enzymes of the carotenoid pathway:**
219 **phytoene desaturases**

220 The most time-consuming tasks in the proposed *in vivo* enzymology protocol are the molecular
221 cloning and strain engineering steps required to generate strains with different substrate
222 concentrations. However, the strains used to investigate a given enzyme can be recycled to
223 investigate downstream steps in the same metabolic pathway, significantly streamlining
224 experiments, which become a simple plug-and-measure process (Fig 5A). Integration of *crtB*,
225 controlled by the high-expression promoter PDC1 into our initial set of strains produced strains with
226 a 430-fold variation in phytoene concentration (from 4 to 1641 µM). These strains thus form an ideal
227 framework to investigate the *in vivo* kinetics of the next metabolic step with various phytoene
228 desaturases.

229 To demonstrate this point, we chose three widely used microbial lycopene-forming phytoene
230 desaturases (1.3.99.31) (22, 23, 25, 26): *P. ananas* CrtI (P21685, PaCrtI), which, along with *Rubrivivax*
231 *gelatinosus* CrtI, is one of only two lycopene-forming phytoene desaturases with published *in vitro*
232 enzymatic parameters (14, 28); and two fungal CrtIs widely used in carotenoid production, one from
233 *Phaffia rhodozyma*, formely *Xanthophyllomyces dendrorhous* (A0A0P0KMF9, XdCrtI), and the other
234 from *Blakeslea trispora* (Q67GI0, BtCrtI), with no enzymatic data available to date.

235 As for the investigation of phytoene synthase, the expression of the phytoene desaturases was
236 controlled by different promoters: TDH3p for PaCrtI, PGK1p for XdCrtI, and PGI1p for BtCrtI. These
237 promoters were chosen based on the relative lycopene producing abilities of the different CrtIs in *S.*
238 *cerevisiae.* This was especially important for BtCrtI, where high expression in the exponential phase
239 caused cell death due to the formation of lycopene crystals (Fig EV2A). PaCrtI and XdCrtI levels did
240 not vary with the phytoene concentration of the strains, but BtCrtI levels were slightly higher in the
241 strains with the lowest phytoene concentrations (Fig EV3). The higher levels of PaCrtI compared with
242 those of the fungal phytoene desaturases is explained in large part by the use of a TDH3 promoter.
243 However, lycopene fluxes were 10 times lower with PaCrtI than with XdCrtI or BtCrtI (Fig 5). Phytoene
244 levels were high enough to saturate both fungal CrtIs (Fig 5) but not PaCrtI, for which lycopene fluxes
245 remained low for all tested phytoene concentrations.

246 The experimental data from the three enzymes were fitted with an irreversible Michaelis-Menten
247 equation, from which $\mathrm{V}_{\mathrm{max}}^{\mathrm{cell}}$ and $K_{1/2}^{\mathrm{cell}}$ values were successfully obtained for XdCrtI and BtCrtI but not
248 for PaCrtI, for which only lower limits for $\mathrm{V}_{\mathrm{max}}^{\mathrm{cell}}$ (13 µM·h^{-1}) and $K_{1/2}^{\mathrm{cell}}$ (560 µM) could be determined
249 (Table EV3). The $\mathrm{V}_{\mathrm{max}}^{\mathrm{cell}}$ values obtained for BtCrtI (309±22 µM·h^{-1}) was higher than for XdCrtI (168±7
250 µM·h^{-1}), and the $K_{1/2}^{\mathrm{cell}}$ for BtCrtI (41±12 µM) was 9 times smaller than XdCrtI's (380±49 µM). The
251 $k_{\mathrm{cat}}^{\mathrm{cell}}$ obtained by integrating quantitative proteomics measurements in strains expressing XdCrtI
252 under PGK1p was 0.030±0.006 s^{-1} (Table EV3).

253 These results highlight the versatility of our approach to compare the *in vivo* behavior of enzymes
254 from different organisms, using the same set of strains, and provide valuable information to
255 understand and optimize natural and synthetic pathways *in vivo*.

256

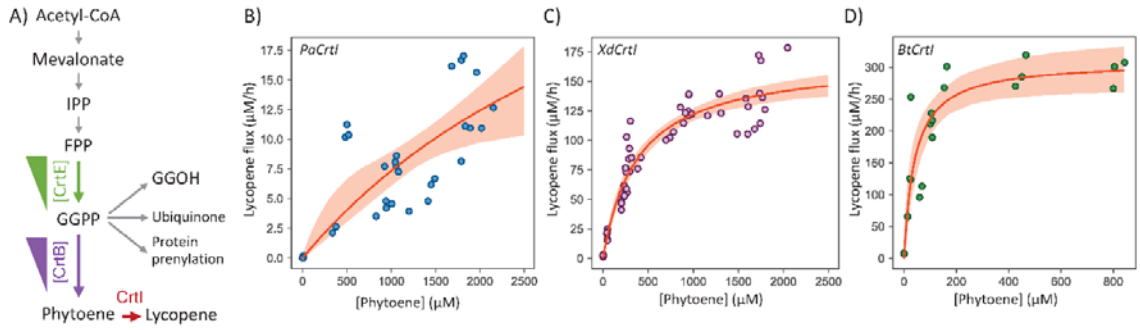

Figure 5. *In vivo* characterization of three phytoene desaturases.

A Scheme for the biosynthesis of lycopene by CrtI.

B–D *In vivo* characterization of CrtI from *P. ananas* (B), *X. dendrorus* (C) and *B. trispora* (D). Each data point represents an independent biological replicate, red lines represent the best fits of a Michaelis-Menten rate law, and shaded areas correspond to 95 % confidence intervals on the fits.

Discussion

Inspired by conventional *in vitro* enzyme assays, we developed an innovative approach to measure enzyme kinetics *in vivo.* We successfully used the proposed method to estimate the *in vivo* equivalents of Michaelis-Menten parameters for a phytoene synthase and two phytoene desaturases in *S. cerevisiae*.

These results highlight the reliability and versatility of our *in vivo* enzymology approach, which hinges on solving two methodological challenges: 1) controlling the substrate pool over a broad concentration range, and 2) measuring the total concentrations of substrate, product and enzyme. The first challenge was addressed using synthetic biology tools to modulate the concentration of a substrate-producing enzyme (here GGPP synthase, CrtE). The second challenge was overcome thanks to sensitive, quantitative metabolomics and proteomics techniques that can be generalized to various other enzymatic models. Indeed, the coverage of the metabolome and fluxome by current omics approaches are now high and are continuously increasing, which enables the application of the proposed approach to a broad range of enzymes. In the absence of absolute quantitative proteomics data, the proposed method still allows for the determination of V_{max}^{cell} and $K_{1/2}^{cell}$ values, providing sufficient information for most enzymology and metabolic engineering studies. Similarly, estimating the absolute $K_{1/2}^{cell}$ values can be achieved using only relative flux values and no absolute concentration of enzymes.

As we advocate for the simplicity of our method, we would like to share some insights on its implementation in future studies. First, to maximize the output of genetic constructs, experimental design should be employed to compare various enzymes that catalyze the same reaction (whether mutants or from different species) or to target multiple enzymes in the same metabolic pathway, in this case phytoene synthase and phytoene desaturase. Second, the number of genetic constructs necessary to reach saturation (ideally 4 to 5) can be minimized by verifying the substrate production range early on. Third, in most cases, testing three enzyme concentrations has been sufficient to obtain a satisfactory saturation curve or at least to precisely estimate the $K_{1/2}^{\mathrm{cell}}$range. Lastly,

290 improvements can be made using high-throughput methods for the construction of plasmids and
291 strains, for growth and for samples preparation steps. The development of single cell metabolomics
292 and proteomics approaches will also significantly increase the throughput of the strain
293 characterization step in future studies. We demonstrate that substrate concentrations can be varied
294 *in vivo* over a wide range. Here, the GGPP concentration was varied by a factor 167 and the phytoene
295 concentration by a factor 430, allowing clear enzyme saturation curves to be observed for the two
296 fungal phytoene desaturases (XdCrtI and BtCrtI). However, while the range of substrate
297 concentrations explored was significantly wider than those used in *in vitro* studies of the same
298 enzymes (Table EV4) (16, 21), complete saturation was not achieved for PaCrtB or PaCrtI. It is
299 conceivable that, when these enzymes are bound to natural membranes, their apparent affinity for
300 the substrate could differ from the *in vitro* environment. A second explanation concerns substrate
301 availability. While classical *in vitro* enzyme assays involve homogeneous, highly diluted buffers, the
302 intracellular environment is dense, heterogeneous and compartmentalized. In this first *in vivo*
303 approach, variations in substrate concentrations between compartments were not considered
304 explicitly, though it may have affected the values obtained for the parameters. For example, a higher
305 concentration of phytoene inside lipid droplets compared with the rest of the membrane would
306 reduce phytoene concentrations around CrtI enzymes and would thus limit substrate saturation.
307 Enzyme localization could also affect measurements as conditions (pH, concentration of ions, etc.)
308 vary between compartments. Iwata-Reuyl et al. found for instance that the measured activity of
309 PaCrtB is 2,000 times lower in the absence of detergents (15), and Fournié et Truan observed that
310 different heterologous CrtI expression systems produced different phytoene saturation patterns (36).
311 In the case of the two *P. ananas* enzymes, the mechanisms that cause the absence of saturation may
312 be different. For PaCrtI, the observed concentrations of phytoene (substrate) and lycopene (product)
313 are either equivalent to or lower than those obtained with the two fungal CrtI enzymes. This suggests
314 a true difference in the affinity for phytoene between the bacterial and fungal enzymes. For PaCrtB,
315 given that the GGPP concentration in the cell is high (around 20 µM), the lack of saturation is more
316 likely due to a heterogeneous distribution of GGPP within the cell, with only a fraction of GGPP being
317 in the vicinity of the enzyme.

318 In addition, other explanations merit attention as they also convey general hypotheses on metabolic
319 systems: i) substrate or product toxicity detrimental to cell growth (e.g. the specific growth rate is
320 nearly 50 % lower for lycopene concentrations above 400 µM, (Fig EV2B), ii) overflow mechanisms
321 that relocate some of the substrate to a different cell compartment or even outside the cell (37, 38),
322 iii) the presence of alternative pathways that divert additional substrate produced above a certain
323 concentration threshold (39, 40), or iv) intrinsic properties of metabolic systems whereby production
324 fluxes tend to decrease when product concentrations increase (41–43). While these mechanisms
325 contribute to global metabolite homeostasis (44–46) and are essential for cell viability, they limit
326 substrate accumulation and thus could prevent complete saturation of the enzyme. Overall, it is
327 crucial to bear in mind that, similarly to *in vitro* data, enzymatic parameters are only valid under the
328 conditions used to measure them. We therefore argue that enzymatic parameters should not be
329 considered constants since they depend on the microenvironment (pH, ion concentration,
330 temperature, membrane composition, etc.), be that *in vitro* or *in vivo*. Still, as mentioned above,
331 these parameters are useful for pathway engineering and an advantage of our *in vivo* enzymology
332 method is that kinetics parameters are measured under the exact same conditions as the enzyme is
333 expressed.

334 It is important to note that various saturation profiles were observed for the tested enzymes,
335 indicating that they may function under very different conditions within the cell. Operating at full
336 saturation (far above the $K_{1/2}^{\mathrm{cell}}$, the enzyme works at its maximum rate, being unaffected by changes
337 in substrate concentration or minor environmental variations. This makes the enzymatic reaction
338 highly robust in terms of product formation. Conversely, if an enzyme operates at substrate
339 concentrations much lower than the $K_{1/2}^{\mathrm{cell}}$, any variation in substrate concentration will directly affect
340 the production rate. This could maintain substrate homeostasis, potentially avoiding toxic effects
341 from concentration changes. From a metabolic engineering perspective, achieving the optimal
342 balance between high product formation and metabolic homeostasis is crucial. This balance can be
343 attained by adjusting the levels of both substrate-forming enzyme and the target enzyme. This
344 process needs to be repeated for each enzyme, potentially under different saturation regimes. In
345 biotechnology, our *in vivo* enzymology approach may thus guide metabolic engineering strategies to
346 ensure that the overall pathway maintains the desired balance between production and cellular
347 homeostasis, thereby ensuring greater stability and robustness of the engineered microbial strains at
348 maximal production flux.

349 The final step in our *in vivo* enzymology method involves fitting experimental data with a
350 mathematical model of enzyme kinetics to obtain the corresponding parameters, the same approach
351 as used in vitro. Traditional enzymatic models were derived with *in vitro* measurements and
352 assumptions in mind. For instance, the classical Michaelis-Menten relationship applies only at steady-
353 state, a condition clearly met in our experimental setup where all data were collected during
354 exponential growth (i.e. metabolite concentrations and fluxes remain constant over time). However,
355 other assumptions do not hold in vivo, in particular regarding the product concentration, which
356 cannot be zero. Nevertheless, for the enzymes investigated here, where the catalyzed reactions are
357 essentially irreversible, the reverse reaction can be neglected, and the Michaelis-Menten formalism
358 still applies. Another important assumption is that the substrate concentration must be higher than
359 the enzyme concentration. In this study, the in vivo substrate/enzyme ratio was between 8 and 1400
360 for PaCrtB and between 2 and 2500 for XdCrtI (Table EV5). Surprisingly, this criterion was not met for
361 CrtB and CrtI in previous in vitro assays (19, 37), with substrate/enzyme ratios between 0.05 and 0.18
362 for PaCrtB and between 1 and 2.57 for PaCrtI (Table EV4). In our setup, despite some formal
363 assumptions not being fully satisfied, the data were still satisfactorily fit with a Michaelis-Menten
364 equation. This underscores the applicability of our method, from which informative parameters such
365 as the degree of saturation can be inferred to understand in vivo enzyme function and to engineer
366 natural and synthetic pathways for biotechnology. The availability of *in vivo* data about enzyme
367 kinetics may also lead to the derivation of specific laws that account for the specificities of in vivo
368 studies (e.g., non-negligible product concentrations).

369 Sixteen years ago, in their review on enzyme function, Dagmar Ringe and Gregory Petsko wrote:
370 "How do enzymes function in a crowded medium of low water activity, where there may be no such
371 thing as a freely diffusing, isolated protein molecule? *In vivo* enzymology is the logical next step along
372 the road that Phillips, Koshland, and their predecessors and successors have traveled so brilliantly so
373 far" (3). The work presented here, albeit performed in the context of a synthetic metabolic pathway,
374 touches on the difference between kinetic parameters measured in vitro and in vivo and their
375 interpretation. We notably show how fine-tuning and balancing the expression of the substrate-
376 producing enzyme and the enzyme under study yields datasets from which meaningful and reliable
377 enzymatic parameters can be obtained. Our method is particularly valuable for studying membrane-

bound and multimeric enzymes, for which the purification and assay optimization steps of classical in vitro enzymology can be extremely challenging. For membrane-bound enzymes, *in vivo* enzymology offers a realistic environment devoid of detergents or other interferences, with natural membranes rather than liposomes. By including additional controlled steps this method could be applied to a wide range of variables, such as inhibition and activation parameters (by modulating the pool of regulatory metabolites) and dynamic data with time-course monitoring in response to metabolic or genetic perturbations, and research questions, such as the effects of cell compartments on enzyme efficiency. New formalisms will be required to account for *in vivo* conditions, notably the presence of products, similar enzyme and substrate concentrations, local concentration variations, and molecular fluxes within the cell. We sincerely hope that our work will stimulate further studies delving deeper into how enzymes function in their natural environment.

391 # Materials and methods

392 ## Plasmid construction

393 Plasmids and primers are listed in Tables EV6-7. Plasmid sequences and annotations are provided in
394 Dataset EV1. The primers were synthesized by IDT (Leuven, Belgium) and the sequences of PaCrtB,
395 PaCrtI and BtCrtI were codon optimized for yeast and synthetized by Twist Bioscience (San Francisco,
396 California). XdCrtE and XdCrtI from *Enterobacter agglomerans* were amplified from pMRI34-CrtE-
397 Gal1-10-HMG1t, YEplac195 YB/I, and pAC-BETA respectively (47–49). Sequences of the mutated
398 versions of the TEF1 promoter TEF1mut2p, TEF1mut5p and TEF1mut7p were obtained from Nevoigt
399 et al. (50). Polymerase chain reaction (PCR) was performed using Phusion high fidelity polymerase
400 and Phire Hot start II DNA polymerase (ThermoFisher Scientific, Lithuania). DNA fragments were
401 purified using Monarch DNA Gel Extraction Kit from New England Biolabs. DNA fragments were
402 annealed by isothermal assembly using NEBuilder HiFi assembly kit from New Englands Biolabs.
403 Clones and plasmids were propagated in homemade calcium- and TOP10-competent *Escherichia coli*
404 cells.

405 ## Construction of yeast strains

406 All yeast strains used in this study are derived from CEN.PK2-1C and are listed in Table EV1. Yeasts
407 were transformed using Gietz et al.'s high-efficiency transformation protocol (51). Integrative
408 cassettes were obtained by enzyme digestion or PCR and were used without any further purification.
409 Strains were selected using auxotrophy markers or antibiotic resistance at a concentration of 400
410 µg/mL. Antibiotic resistance recycling was performed using vector pSH63 as described in the
411 literature (52). Genome integration was verified by colony PCR using the primers listed in Table EV7.
412 Genomic DNA was extracted using DNA release from ThermoFisher Scientific.

413 ## Media and culture conditions

414 All strains were grown in modified synthetic Verduyn media containing glucose (111 mM), NH_4Cl (75
415 mM), KH_2PO_4 (22 mM), $MgSO_4$ (0.4 mM) and CSM (ForMedium LTD, Hunstaton, England) at pH 5.0
416 (53). Sterilization was performed by filtration. Fresh colonies from selective plates were precultured
417 in 350 µL complete synthetic medium at 28 °C for 8 hours and these cells were used to inoculate
418 cultures with a 1:5 medium:flask proportion to an initial OD_{600nm} of 0.002, grown at 200 rpm at 28 °C.

419 ## Carotene quantification

420 Samples (10 or 20 mL) of yeast culture were harvested with an OD_{600nm} of approximately 5,
421 centrifuged, and washed with 1 mL of MilliQ water. Cell pellets were freeze-dried and stored at –80
422 °C until extracted. β-apocarotenal solution (40 µL, 50 µM) was added to the dried cells, and
423 carotenes were extracted with glass beads and 500 µL of acetone in three 20 s rounds of agitation at
424 0.05 m/s with a FastPrep FP120 cell disruptor (ThermoFisher). The acetone phase was transferred to
425 a new tube and the extraction was repeated twice. Acetone extracts were pooled, centrifuged, dried
426 under nitrogen flux, and resuspended in acetone for HPLC analysis. Analyses were carried out on a
427 Thermo Scientific Vanquish Focused UHPLC Plus system with DAD HL. Extract samples (5 µL) were
428 injected into a YMC carotenoid column (100 × 2.0 mm and 3 µm particle size) equipped with a
429 precolumn (100 × 2.0 mm and 3 µm particle size). The mobile phases used to separate and quantify
430 phytoene, lycopene and β-apocarotenal from ergosterol and derivatives were mixtures of (A)
431 methanol/water (95:5) and (B) dichloromethane. The flow was 0.25 mL/min with the following

432 gradient: 0–0.1 min 5 % B, 0.1–0.5 min 20 % B, 0.5–2 min 60 % B, 2–5 min 80 % B, 5–8 min 80 % B
433 and 8–11 min 5 % B. The absorbance from 210 to 600 nm was measured throughout the run with a
434 data collection rate of 2 Hz and a response time of 2 s. The phytoene concentration was deduced
435 from its absorbance at 286 nm and lycopene and β-apocarotenal concentrations from the
436 absorbance at 478 nm. The reference wavelength (600 nm) was subtracted from each of the
437 wavelengths used for metabolite quantification.

438 **Flux calculation**

439 Phytoene and lycopene are produced and accumulate in the cells, and their pools are continuously
440 diluted by cell growth. Assuming an absence of degradation or reutilization of these end-products by
441 the cell, phytoene and lycopene production fluxes are balanced solely by their dilution fluxes in the
442 exponential growth phase, where cells are at metabolic steady-state. Thus, phytoene and lycopene
443 production fluxes were determined by multiplying their concentrations by the cell growth rate. This
444 flux calculation method provides results consistent with those obtained by targeted ^{13}C-fluxomics
445 (54).

446 **GGPP quantification**

447 GGPP was quantified as detailed previously (55). Briefly, 10 mL of broth was filtered through 0.45 µm
448 Sartolon polyamide (Sartorius, Goettingen, Germany) and washed with 5 mL of fresh culture medium
449 (without glucose). The filters were rapidly plunged into liquid nitrogen and then stored at −80 °C until
450 extraction. Intracellular GGPP was extracted by incubating filters in closed glass tubes containing 5
451 mL of an isopropanol/H_20 NH_4HCO_3 100 mM (50/50) mixture at 70 °C for 10 min. For absolute GGPP
452 quantification, 50 µL of ^{13}C internal standard were added to each extract. Cellular extracts were
453 cooled on ice and sonicated for 1 min. Cell debris was removed by centrifugation (5000 g, 4 °C, 5
454 min). Supernatants were evaporated overnight (SC110A SpeedVac Plus, ThermoFisher, Waltham,
455 MA, USA), resuspended in 200 µL of methanol:NH_4OH 10 mM (7:3) at pH 9.5 and stored at −80 °C
456 until analysis.

457 Analyses were carried out on a LC–MS platform composed of a Thermo Scientific Vanquish Focused
458 UHPLC Plus system with DAD HL, coupled to a Thermo Scientific Q Exactive Plus hybrid quadrupole-
459 Orbitrap mass spectrometer (ThermoFisher), as detailed previously (55). Calibration mixtures
460 (prepared at concentrations from 0.08 nM to 10 µM) were used to construct calibration curves from
461 which the absolute concentration of GGPP in the samples was determined.

462 **Western blot**

463 Protein extracts were prepared as described by Zhang et al. (46). Briefly, 1.5 OD_{600nm} of pelleted cells
464 were pre-treated with 100 µL of a 2 M lithium acetate cold solution, and left to stand for 5 min,
465 followed by 5 min centrifugation at 5000 g, 4 °C. The supernatant was discarded and 100 µL of a
466 0.4 M solution of NaOH was added. After gentle resuspension, and 5 min standing on ice, the
467 samples were centrifuged for 5 min at 4 °C. After discarding supernatants, the pellets were
468 vigorously vortexed with 60 µL of bromophenol blue loading dye solution with 5 % β-
469 mercaptoethanol. After denaturation for 10 min at 99 °C, 5 µL of each sample was loaded onto 10
470 % SDS page gel. Semi-dry transfer was performed on PVDF membrane (Merck Millipore, Darmstadt,
471 Germany) using a Trans-Blot SD Cell BioRad apparatus (18 V during 20 min), and 5 % bovine milk in
472 TBS as blocking agent. Incubations were performed with mouse anti-FLAG or mouse anti-V5
473 (ThermoFisher Scientific), and secondary anti-mouse IgG coupled with horseradish peroxidase

474 (ThermoFisher Scientific), diluted according to manufacturer instructions. Proteins were detected by
475 incubation with SuperSignal West Pico PLUS substrate (ThermoFisher Scientific).

476 **Proteomics**

477 For cell disruption, 10^8 cells were dissolved in 200 µL of lysis buffer (0.1 M NaOH, 2 % SDS, 2 % 2-
478 mercaptoethanol, 0.05 M EDTA), heated at 90 °C for 10 min and neutralized with 5 µL of 4 M acetic
479 acid. Glass beads were added and the samples were vortexed at 4 °C for 30 min. Cell debris was
480 pelleted by centrifugation and 3000 g for 10 min and the protein concentration of the supernatant
481 was determined using the Bradford assay. Protein aliquots (400 µg) were cleaned by methanol
482 chloroform precipitation. The protein samples were dissolved in 5 µL of 6 M guanidinium chloride, 5
483 µL of 0.1 M dithiothreitol (DTT), and 100 µL of 50 mM TEAB 50 and diluted to a protein concentration
484 of 2 µg/µL with 90 µL of water. Absolute protein quantification was performed using heavy isotope
485 labeled tryptic peptides as internal standards. Protein lysate aliquots (20 µg) were spiked with a
486 mixture of ten AQUA peptides, C-terminally labeled with heavy lysine or arginine (ThermoFisher
487 Scientific) with concentrations of 50 fmol/µg, 10 fmol/µg, 5 fmol/µg and 0 fmol/µg. The samples
488 were reduced by adding 2 µL of 0.1 M DTT and incubating at 60 °C for 1 h, alkylated with 2 µL of
489 chloroacetamide 0.5 M at room temperature for 30 min, and digested with 0.5 µg of trypsin
490 overnight. Digestion was stopped by adding 5 µL of 1 % TFA and the samples were cleaned using 100
491 µL C18 tips. The extracts were lyophilized, reconstituted in 20 µL of eluent A, and transferred to HPLC
492 vials.

493 Samples were analyzed in triplicate using an UltiMate 3000 UHLC system coupled to a Q Exactive Plus
494 mass spectrometer (ThermoFisher Scientific). Approximately 0.6 µg of peptides were loaded on a C18
495 precolumn (PepMap100, 5 µm, 300 Å, ThermoFisher Scientific) and separated on a PepMap RSLC C18
496 column (50 cm × 75 µm, 2 µm, 100 Å, ThermoFisher Scientific) with a 1.5 h gradient with eluent A
497 (Water, 0.05 % FA) and eluent B (80 % ACN, 0.04 % FA) with a flow rate of 0.3 µL/min. The peptides
498 were first desalted for 4 min at 5 % B, then separated with a gradient to 50 % B over 65 min, to 90 %
499 B in 3 min, held at 90 % B for 8 min, and then equilibrated for 8 min at 4 % B.

500 For targeted absolute quantification, full MS spectra measurements were followed by parallel
501 reaction monitoring (PRM) of targeted heavy AQUA peptides and the corresponding light, native
502 peptide of the proteins of interest. The full MS spectra were acquired in profile mode with the
503 following settings: resolution of 70000, mass range of 350–950 m/z, AGC target of 10^6, and 80 ms
504 maximum injection time. PRM MS2 spectra were acquired with an isolation window of 1.6 m/z,
505 17500 resolution, AGC target of 10^5, 80 ms injection time, and an NCE of 27. The inclusion list
506 contained 26 entries covering the light and heavy species of 10 peptides at the most intense charge
507 state (2+ or 3+).

508 Database searches were performed with Proteome Discoverer (version 3.01.27; ThermoFisher). The
509 raw data were compared with the UniProt protein databases of *S. cerevisiae* strain CEN.PK113-7D
510 (UniProt 02.2023; 5,439 entries), and common contaminants using Sequest HT and Chimerys search
511 algorithms. The Sequest search parameters were a semi-tryptic protease specificity with a maximum
512 of 2 missed cleavage sites. The precursor mass tolerance was 8 ppm and the fragment mass
513 tolerance was 0.02 Da. Oxidation of methionine and acetylation of protein N-termini were allowed as
514 dynamic modifications. Carbamidomethylation of cysteine was set as a static modification. Chimerys
515 database searches were performed with default settings. Percolator q-values were used to restrict

the false discovery rate (FDR) of peptide spectrum matches to 0.01. The FDR of peptide and protein identifications was restricted to 1 % and strict parsimony principles were applied to protein grouping.

A spectral library of the AQUA peptides was generated using Proteome Discoverer with a sample containing only 500 fmol of the ten AQUA peptides, in addition to the PRM analyses of the spiked yeast samples. The PRM data of three concentrations analyzed in triplicate were imported and all transitions were reviewed using Skyline (57). Between four and nine transitions without interference were chosen for each peptide and the ratio of light and heavy peptides of the sum of transitions was calculated for absolute quantification. The list of used peptides and all corresponding transitions are provided in Table EV8.

Calculation of absolute concentrations

Protein and metabolite concentrations are expressed as absolute intracellular concentrations. Metabolite concentrations initially expressed in µmol/g DCW were converted into absolute intracellular concentrations using a conversion factor of 6.59×10^{10} cells/g DCW (Fig EV4) and a cellular volume of 66 μm^3 (58). The intracellular concentrations of PaCrtB and XdCrtI were calculated using a conversion factor of 0.63 g protein/g DCW for yeast grown on ammonium sulfate medium (59). All calculations for data conversion are provided in the corresponding Extended view Tables.

Modeling

To test the impact of enzyme expression level on the obtained kinetic profiles, we built a toy kinetic model of the pathway under study. This model contains two metabolites (GGPP and phytoene) and three reactions: GGPP formation by CrtE, defined as a constant flux; GGPP conversion into phytoene by CrtB, modelled using a Michaelis-Menten rate law; and phytoene dilution by growth, modelled using mass action. The K_M value of CrtB was set arbitrarily to 1, and we simulated the steady-state phytoene production flux and GGPP concentration for three CrtB levels (V_{max} set to 0.02, 0.4 and 0.7) under a broad range of GGPP-producing flux (from 0.01 to 0.4 µM/h). The model has been developed with COPASI v4.39 (60) and is available from our GitHub repository (https://github.com/MetaSys-LISBP/in_vivo_enzymatic_parameters) and from the Biomodels database (61) under accession ID MODEL2407240001. All simulations were performed with COPASI.

Calculation of enzyme parameters

Enzymatic parameters (V_{max} and K_M) were determined by fitting a Michaelis-Menten equation to the measured relationships between substrate concentrations and reaction rates. Uncertainties on fitted parameters were determined using a Monte-Carlo approach. Briefly, 1000 simulated noisy datasets were generated (where the noise was determined as the standard deviation of residuals obtained for the fit of the experimental dataset), and the mean value, standard deviation, and 95 % confidence intervals of each parameter were determined from the distribution of values obtained for the 1000 datasets. For each enzyme, we verified that all parameters were identifiable based on the covariance matrix and on the results of the Monte-Carlo analysis. The code for parameter estimation and statistical analysis is provided as a Jupyter notebook at https://github.com/MetaSys-LISBP/in_vivo_enzymatic_parameters.

Data Availability

The data used to make the figures can be found in the Source Data files. The model and computer code produced in this study are available in the following databases:

- Model: BioModels MODEL2407240001 (https://www.ebi.ac.uk/biomodels/MODEL2407240001)
- Code: GitHub (https://github.com/MetaSys-LISBP/in_vivo_enzymatic_parameters)

Acknowledgements

The authors thank MetaboHub-MetaToul (Metabolomics & Fluxomics facilities, Toulouse, France, https://mth-metatoul.com), which is part of the French National Infrastructure for Metabolomics and Fluxomics (https://www.metabohub.fr), funded by the ANR (MetaboHUB-ANR-11-INBS-0010), for access to MS facilities. The authors also thank Jean-Charles Portais (RESTORE, Geroscience & Rejuvenation Center, Université de Toulouse, INSERM, CNRS, EFS, Toulouse, France), Sylvie Dequin (SPO, Université Montpellier, INRAE, Institut Agro Montpellier, Montpellier, France), Thibault Nidelet (SPO, Université Montpellier, INRAE, Institut Agro Montpellier, Montpellier, France), Thomas Lautier (TBI, Université de Toulouse, CNRS, INRAE, INSA, Toulouse, France) and Sergueï Sokol (TBI, Université de Toulouse, CNRS, INRAE, INSA, Toulouse, France) for insightful discussions.

Competing interests

The authors declare no competing interests.

Funding

This work was supported by the French National Research Agency project ENZINVIVO (ANR-16-CE11-0022).

Contributions

Funding acquisition: CC, SH, PM, GT; Project administration: CC, SH, GT; Conceptualization: CC, SCC, SH, PM, GT; Investigation: SCC, AC, HK, CT, AT, VG, CC, PM; Methodology: SCC, AC, HB, CT, FB, AT, VG, CC, SH, LGA, PM, GT; Software: PM; Formal Analysis: SCC, AC, HB, CT, AT, LGA, PM, GT; Visualization: SCC, PM, GT; Writing – original draft: SCC, PM, GT; Writing – review & editing: SCC, AC, HB, CT, FB, AT, VG, CC, SH, LGA, PM, GT; Supervision: SCC, VG, PM, GT.

585 ## References

586 1. S. R. McGuffee, A. H. Elcock, Diffusion, Crowding & Protein Stability in a Dynamic Molecular
587 Model of the Bacterial Cytoplasm. *PLOS Computational Biology* **6**, e1000694 (2010).
588 2. B. M. B. Karen van Eunen, The importance and challenges of in vivo-like enzyme kinetics.
589 *Perspectives in Science* **1**, 126–130 (2014).
590 3. D. Ringe, G. A. Petsko, How Enzymes Work. *Science* **320**, 1428–1429 (2008).
591 4. A. Sancar, Structure and Function of Photolyase and in Vivo Enzymology: 50th Anniversary. *J.*
592 *Biol. Chem.* **283**, 32153–32157 (2008).
593 5. W. Harm, H. Harm, C. S. Rupert, Analysis of photoenzymatic repair of UV lesions in DNA by
594 single light flashes: II. In vivo studies with Escherichia coli cells and bacteriophage. *Mutation*
595 *Research/Fundamental and Molecular Mechanisms of Mutagenesis* **6**, 371–385 (1968).
596 6. B. E. Wright, M. H. Butler, K. R. Albe, Systems analysis of the tricarboxylic acid cycle in
597 Dictyostelium discoideum. I. The basis for model construction. *Journal of Biological Chemistry*
598 **267**, 3101–3105 (1992).
599 7. D. Heckmann, *et al.*, Kinetic profiling of metabolic specialists demonstrates stability and
600 consistency of in vivo enzyme turnover numbers. *Proc Natl Acad Sci USA* 202001562 (2020).
601 https://doi.org/10.1073/pnas.2001562117.
602 8. D. Davidi, *et al.*, Global characterization of in vivo enzyme catalytic rates and their
603 correspondence to in vitro k_{cat} measurements. *Proc Natl Acad Sci USA* **113**, 3401–3406 (2016).
604 9. A. Zotter, F. Bäuerle, D. Dey, V. Kiss, G. Schreiber, Quantifying enzyme activity in living cells. *J*
605 *Biol Chem* **292**, 15838–15848 (2017).
606 10. S. Bhattacharyya, S. Bershtein, B. V. Adkar, J. Woodard, E. I. Shakhnovich, Metabolic response
607 to point mutations reveals principles of modulation of in vivo enzyme activity and phenotype.
608 *Mol Syst Biol* **17**, e10200 (2021).
609 11. Y. Takakuwa, H. Nishino, Y. Ishibe, T. Ishibashi, Properties and kinetics of membrane-bound
610 enzymes when both the enzyme and substrate are components of the same microsomal
611 membrane. Studies on lathosterol 5-desaturase. *Journal of Biological Chemistry* **269**, 27889–
612 27893 (1994).
613 12. M. Camagna, *et al.*, Enzyme Fusion Removes Competition for Geranylgeranyl Diphosphate in
614 Carotenogenesis. *Plant Physiol.* **179**, 1013–1027 (2019).
615 13. P. Urban, *et al.*, Engineered yeasts simulating P450-dependent metabolisms: tricks, myths and
616 reality. *Drug Metabol Drug Interact* **11**, 169–200 (1994).
617 14. S. Gemmecker, *et al.*, Phytoene Desaturase from Oryza sativa: Oligomeric Assembly, Membrane
618 Association and Preliminary 3D-Analysis. *PLoS One* **10**, e0131717 (2015).
619 15. D. Iwata-Reuyl, S. K. Math, S. B. Desai, C. D. Poulter, Bacterial Phytoene Synthase:? Molecular
620 Cloning, Expression, and Characterization of Erwinia herbicola Phytoene Synthase†.
621 *Biochemistry* **42**, 3359–3365 (2003).
622 16. P. Schaub, *et al.*, On the Structure and Function of the Phytoene Desaturase CRTI from Pantoea
623 ananatis, a Membrane-Peripheral and FAD-Dependent Oxidase/Isomerase. *PLoS ONE* **7**, e39550
624 (2012).
625 17. M. Fournié, G. Truan, Multiplicity of carotene patterns derives from competition between
626 phytoene desaturase diversification and biological environments. *Sci Rep* **10**, 21106 (2020).
627 18. P. Stickforth, G. Sandmann, Structural and kinetics properties of a mutated phytoene
628 desaturase from Rubrivivax gelatinosus with modified product specificity. *Arch Biochem*
629 *Biophys* **505**, 118–122 (2011).
630 19. L. Michaelis, M. Menten, Die Kinetik der Invertinwirkung. *Biochemische Zeitschrift* **49**, 333–369
631 (1913).
632 20. F. J. Bruggeman, J. J. Hornberg, F. C. Boogerd, H. V. Westerhoff, Introduction to systems
633 biology. *EXS* **97**, 1–19 (2007).

21. U. Neudert, I. M. Martínez-Férez, P. D. Fraser, G. Sandmann, Expression of an active phytoene synthase from Erwinia uredovora and biochemical properties of the enzyme. *Biochimica et Biophysica Acta (BBA) - Lipids and Lipid Metabolism* **1392**, 51–58 (1998).
22. P. D. Fraser, W. Schuch, P. M. Bramley, Phytoene synthase from tomato (Lycopersicon esculentum) chloroplasts – partial purification and biochemical properties. *Planta* **211**, 361–369 (2000).
23. B. Camara, "[32] Plant phytoene synthase complex: Component enzymes, immunology, and biogenesis" in *Methods in Enzymology*, Carotenoids Part B: Metabolism, Genetics, and Biosynthesis., (Academic Press, 1993), pp. 352–365.
24. A. Schofield, G. Paliyath, Modulation of carotenoid biosynthesis during tomato fruit ripening through phytochrome regulation of phytoene synthase activity. *Plant Physiology and Biochemistry* **43**, 1052–1060 (2005).
25. G. Sandmann, Evolution of carotene desaturation: The complication of a simple pathway. *Archives of Biochemistry and Biophysics* **483**, 169–174 (2009).
26. J. Koschmieder, *et al.*, Plant-type phytoene desaturase: Functional evaluation of structural implications. *PLoS ONE* **12**, e0187628 (2017).
27. H. Rabeharindranto, *et al.*, Enzyme-fusion strategies for redirecting and improving carotenoid synthesis in *S. cerevisiae*. *Metab Eng Commun* **8**, e00086 (2019).
28. Y. Chen, *et al.*, Lycopene overproduction in *Saccharomyces cerevisiae* through combining pathway engineering with host engineering. *Microbial Cell Factories* **15**, 113 (2016).
29. P. J. Westfall, *et al.*, Production of amorphadiene in yeast, and its conversion to dihydroartemisinic acid, precursor to the antimalarial agent artemisinin. *PNAS* **109**, E111–E118 (2012).
30. J. Zhao, *et al.*, Dynamic control of ERG20 expression combined with minimized endogenous downstream metabolism contributes to the improvement of geraniol production in *Saccharomyces cerevisiae*. *Microb Cell Fact* **16**, 1–11 (2017).
31. A. Faulkner, *et al.*, The LPP1 and DPP1 Gene Products Account for Most of the Isoprenoid Phosphate Phosphatase Activities inSaccharomyces cerevisiae. *J. Biol. Chem.* **274**, 14831–14837 (1999).
32. B. Peng, L. K. Nielsen, S. C. Kampranis, C. E. Vickers, Engineered protein degradation of farnesyl pyrophosphate synthase is an effective regulatory mechanism to increase monoterpene production in Saccharomyces cerevisiae. *Metabolic Engineering* **47**, 83–93 (2018).
33. C. Chambon, V. Ladeveze, A. Oulmouden, M. Servouse, F. Karst, Isolation and properties of yeast mutants affected in farnesyl diphosphate synthetase. *Curr Genet* **18**, 41–46 (1990).
34. K. Tokuhiro, *et al.*, Overproduction of Geranylgeraniol by Metabolically Engineered Saccharomyces cerevisiae. *Appl. Environ. Microbiol.* **75**, 5536–5543 (2009).
35. X. Zhou, *et al.*, Phytoene Synthase: The Key Rate-Limiting Enzyme of Carotenoid Biosynthesis in Plants. *Frontiers in Plant Science* **13** (2022).
36. D. Leys, J. Basran, F. Talfournier, M. J. Sutcliffe, N. S. Scrutton, Extensive conformational sampling in a ternary electron transfer complex. *Nat Struct Mol Biol* **10**, 219–225 (2003).
37. L. Phégnon, *et al.*, Phosphogluconolactonase as the linchpin of an efficient pentose phosphate pathway. [Preprint] (2023). Available at: https://www.biorxiv.org/content/10.1101/2023.11.29.569206v2 [Accessed 8 December 2023].
38. J. O. Park, *et al.*, Metabolite concentrations, fluxes and free energies imply efficient enzyme usage. *Nat Chem Biol* **12**, 482–489 (2016).
39. X. Bu, J. Lin, C. Duan, M. A. G. Koffas, G. Yan, Dual regulation of lipid droplet-triacylglycerol metabolism and ERG9 expression for improved β-carotene production in Saccharomyces cerevisiae. *Microb Cell Fact* **21**, 3 (2022).
40. Y. Zhu, *et al.*, Enhanced synthesis of Coenzyme Q10 by reducing the competitive production of carotenoids in Rhodobacter sphaeroides. *Biochemical Engineering Journal* **125**, 50–55 (2017).
41. R. Heinrich, T. A. Rapoport, A linear steady-state treatment of enzymatic chains. General properties, control and effector strength. *Eur J Biochem* **42**, 89–95 (1974).

42. H. Kacser, J. A. Burns, The control of flux. *Symp Soc Exp Biol* **27**, 65–104 (1973).
43. B. Enjalbert, P. Millard, M. Dinclaux, J.-C. Portais, F. Létisse, Acetate fluxes in Escherichia coli are determined by the thermodynamic control of the Pta-AckA pathway. *Sci Rep* **7**, 42135 (2017).
44. S.-M. Fendt, *et al.*, Tradeoff between enzyme and metabolite efficiency maintains metabolic homeostasis upon perturbations in enzyme capacity. *Mol Syst Biol* **6**, 356 (2010).
45. P. Millard, K. Smallbone, P. Mendes, Metabolic regulation is sufficient for global and robust coordination of glucose uptake, catabolism, energy production and growth in Escherichia coli. *PLOS Computational Biology* **13**, e1005396 (2017).
46. M. L. Reaves, B. D. Young, A. M. Hosios, Y.-F. Xu, J. D. Rabinowitz, Pyrimidine homeostasis is accomplished by directed overflow metabolism. *Nature* **500**, 237–241 (2013).
47. R. Verwaal, *et al.*, High-Level Production of Beta-Carotene in Saccharomyces cerevisiae by Successive Transformation with Carotenogenic Genes from Xanthophyllomyces dendrorhous. *Appl. Environ. Microbiol.* **73**, 4342–4350 (2007).
48. F. X. Cunningham Jr, *et al.*, Functional analysis of the beta and epsilon lycopene cyclase enzymes of Arabidopsis reveals a mechanism for control of cyclic carotenoid formation. *The Plant Cell* **8**, 1613–1626 (1996).
49. W. Xie, *et al.*, Construction of a controllable β-carotene biosynthetic pathway by decentralized assembly strategy in Saccharomyces cerevisiae. *Biotechnol. Bioeng.* **111**, 125–133 (2014).
50. Engineering of Promoter Replacement Cassettes for Fine-Tuning of Gene Expression in Saccharomyces cerevisiae | Applied and Environmental Microbiology. Available at: https://journals-asm-org.insb.bib.cnrs.fr/doi/10.1128/aem.00530-06 [Accessed 30 January 2024].
51. R. D. Gietz, Yeast transformation by the LiAc/SS carrier DNA/PEG method. *Methods Mol. Biol.* **1205**, 1–12 (2014).
52. U. Güldener, S. Heck, T. Fiedler, J. Beinhauer, J. H. Hegemann, A New Efficient Gene Disruption Cassette for Repeated Use in Budding Yeast. *Nucl. Acids Res.* **24**, 2519–2524 (1996).
53. C. Verduyn, E. Postma, W. A. Scheffers, J. P. Y. 1990 van Dijken, Physiology of Saccharomyces Cerevisiae in Anaerobic Glucose-Limited Chemostat Culturesx. *Microbiology* **136**, 395–403.
54. P. Millard, *et al.*, ScalaFlux: A scalable approach to quantify fluxes in metabolic subnetworks. *PLOS Computational Biology* **16**, e1007799 (2020).
55. S. Castaño-Cerezo, *et al.*, Functional analysis of isoprenoid precursors biosynthesis by quantitative metabolomics and isotopologue profiling. *Metabolomics* **15**, 115 (2019).
56. T. Zhang, *et al.*, An improved method for whole protein extraction from yeast Saccharomyces cerevisiae. *Yeast* **28**, 795–798 (2011).
57. B. MacLean, *et al.*, Effect of Collision Energy Optimization on the Measurement of Peptides by Selected Reaction Monitoring (SRM) Mass Spectrometry. *Anal. Chem.* **82**, 10116–10124 (2010).
58. N. Punekar, "In Vitro Versus In Vivo: Concepts and Consequences" in *ENZYMES: Catalysis, Kinetics and Mechanisms*, Springer Singapore, (2018), pp. 493–519.
59. E. Albers, C. Larsson, G. Lidén, C. Niklasson, L. Gustafsson, Influence of the nitrogen source on *Saccharomyces cerevisiae* anaerobic growth and product formation. *Appl Environ Microbiol* **62**, 3187–3195 (1996).
60. COPASI—a COmplex PAthway SImulator | Bioinformatics | Oxford Academic. Available at: https://academic.oup.com/bioinformatics/article/22/24/3067/208398 [Accessed 25 July 2024].
61. R. S. Malik-Sheriff, *et al.*, BioModels—15 years of sharing computational models in life science. *Nucleic Acids Research* **48**, D407–D415 (2020).

Expanded View Figure legends

Figure EV1. PaCrtB-FLAG expression determined by western blot in yeast strains with different GGPP concentrations (panels A, B and C correspond to three different biological replicates).

Figure EV2. Lycopene production in *S. cerevisiae*.

A *S. cerevisiae* yGGPP34 strain expressing PDC1p-PaCrtB and TDH3p-BtCrtI. Bright field images were acquired using the camera LEICA DFC300FX mounted in the microscope Leica DM4000B with Leica EL6000 light source. Lycopene crystals are observed in red.

B Decrease of specific growth rate in yeast strains expressing BtCrtI with different phytoene concentrations.

Figure EV3. Expression of the three studied CrtI-V5 proteins in strains with low (yGGPP030) and high (yGGPP044) phytoene content (panels A and B correspond to three different biological replicates).

Figure EV4. Correlation between cell/mL and OD_{600nm} (A) and between OD_{600nm} and mg DCW (B).

Expanded View Table legends

Table EV1. Yeast strains used in this study.

Table EV2. PaCrtB and XdCrtI absolute protein quantification.

Table EV3. Enzymatic parameters measured *in vivo*.

Table EV4. *In vitro* parameters of bacterial phytoene synthase and phytoene desaturase.

Table EV5. Molecule number of each component for the *in vivo* enzymology reaction.

Table EV6. Plasmids used in this study.

Table EV7. Primers used for colony PCRs.

Table EV8. Peptides and PRM transitions used for absolute quantification of the enzymes.

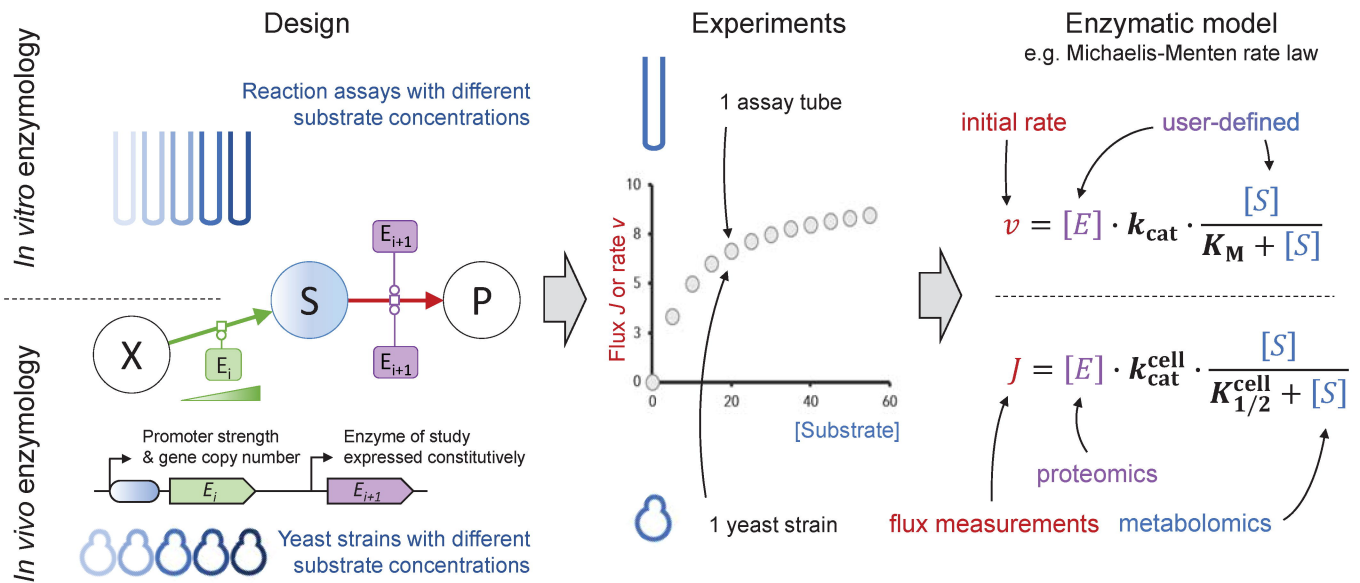
Design
Experiments
Enzymatic model
e.g. Michaelis-Menten rate law
In vitro enzymology
Reaction assays with different substrate concentrations
X
S
P
E_i
E_{i+1}
E_{i+1}
1 assay tube
Flux J or rate v
[Substrate]
initial rate
user-defined
$v = [E] \cdot k_{cat} \cdot \frac{[S]}{K_M + [S]}$
In vivo enzymology
Promoter strength & gene copy number
Enzyme of study expressed constitutively
E_i
E_{i+1}
Yeast strains with different substrate concentrations
1 yeast strain
$J = [E] \cdot k_{cat}^{cell} \cdot \frac{[S]}{K_{1/2}^{cell} + [S]}$
proteomics
flux measurements
metabolomics

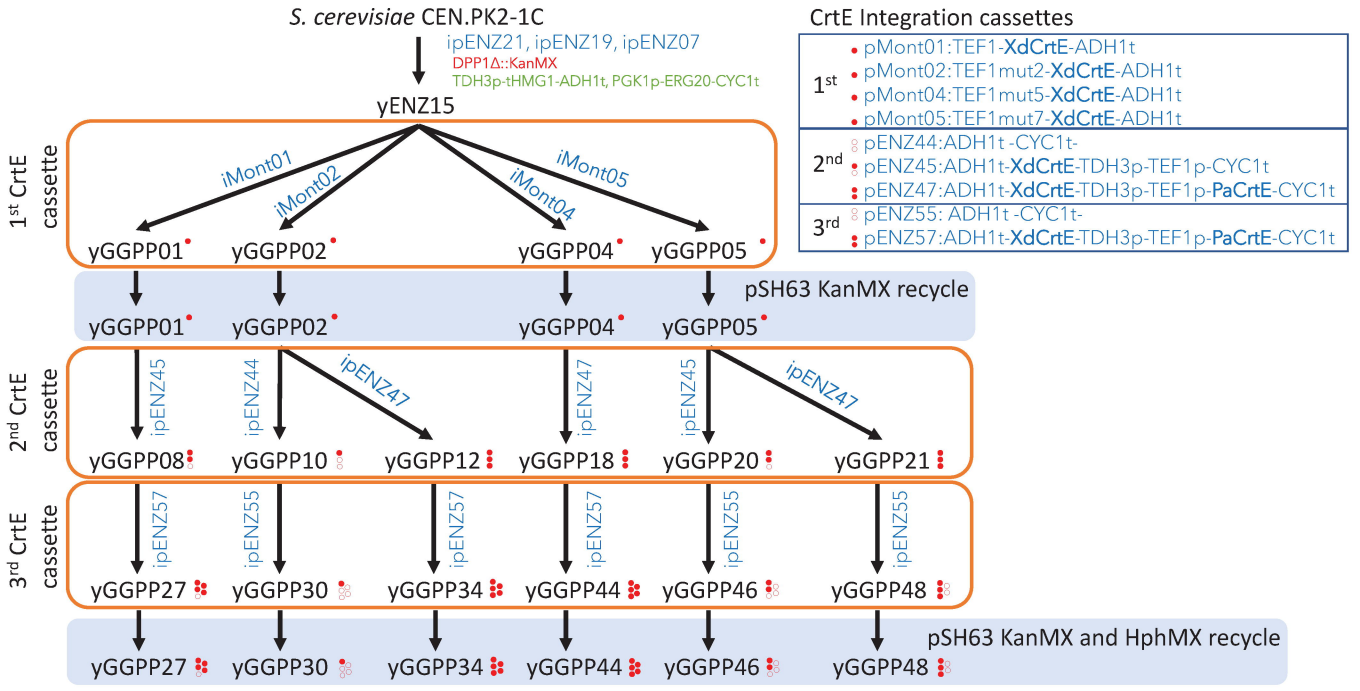
S. cerevisiae CEN.PK2-1C
ipENZ21, ipENZ19, ipENZ07
DPP1Δ::KanMX
TDH3p-tHMG1-ADH1t, PGK1p-ERG20-CYC1t
yENZ15
1st CrtE cassette
iMont01
iMont02
iMont04
iMont05
yGGPP01
yGGPP02
yGGPP04
yGGPP05
pSH63 KanMX recycle
yGGPP01
yGGPP02
yGGPP04
yGGPP05
2nd CrtE cassette
ipENZ45
ipENZ44
ipENZ47
ipENZ47
ipENZ45
ipENZ47
yGGPP08
yGGPP10
yGGPP12
yGGPP18
yGGPP20
yGGPP21
3rd CrtE cassette
ipENZ57
ipENZ55
ipENZ57
ipENZ57
ipENZ55
ipENZ55
yGGPP27
yGGPP30
yGGPP34
yGGPP44
yGGPP46
yGGPP48
pSH63 KanMX and HphMX recycle
yGGPP27
yGGPP30
yGGPP34
yGGPP44
yGGPP46
yGGPP48
CrtE Integration cassettes
1st
pMont01:TEF1-XdCrtE-ADH1t
pMont02:TEF1mut2-XdCrtE-ADH1t
pMont04:TEF1mut5-XdCrtE-ADH1t
pMont05:TEF1mut7-XdCrtE-ADH1t
2nd
pENZ44:ADH1t -CYC1t-
pENZ45:ADH1t-XdCrtE-TDH3p-TEF1p-CYC1t
pENZ47:ADH1t-XdCrtE-TDH3p-TEF1p-PaCrtE-CYC1t
3rd
pENZ55: ADH1t -CYC1t-
pENZ57:ADH1t-XdCrtE-TDH3p-TEF1p-PaCrtE-CYC1t

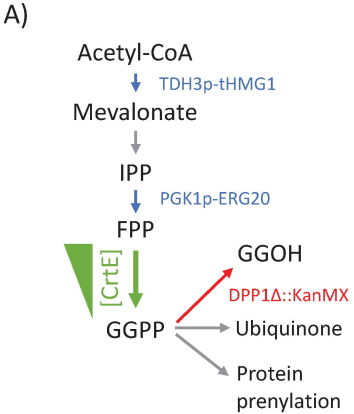
A)
Acetyl-CoA
TDH3p-tHMG1
Mevalonate
IPP
PGK1p-ERG20
FPP
[CrtE]
GGOH
DPP1Δ::KanMX
GGPP
Ubiquinone
Protein
prenylation

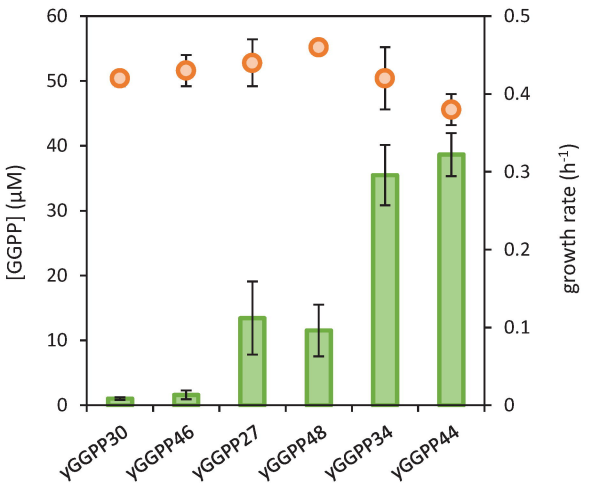
B)
[GGPP] (μM)
growth rate (h-1)
0
10
20
30
40
50
60
0
0.1
0.2
0.3
0.4
0.5
yGGPP30
yGGPP46
yGGPP27
yGGPP48
yGGPP34
yGGPP44

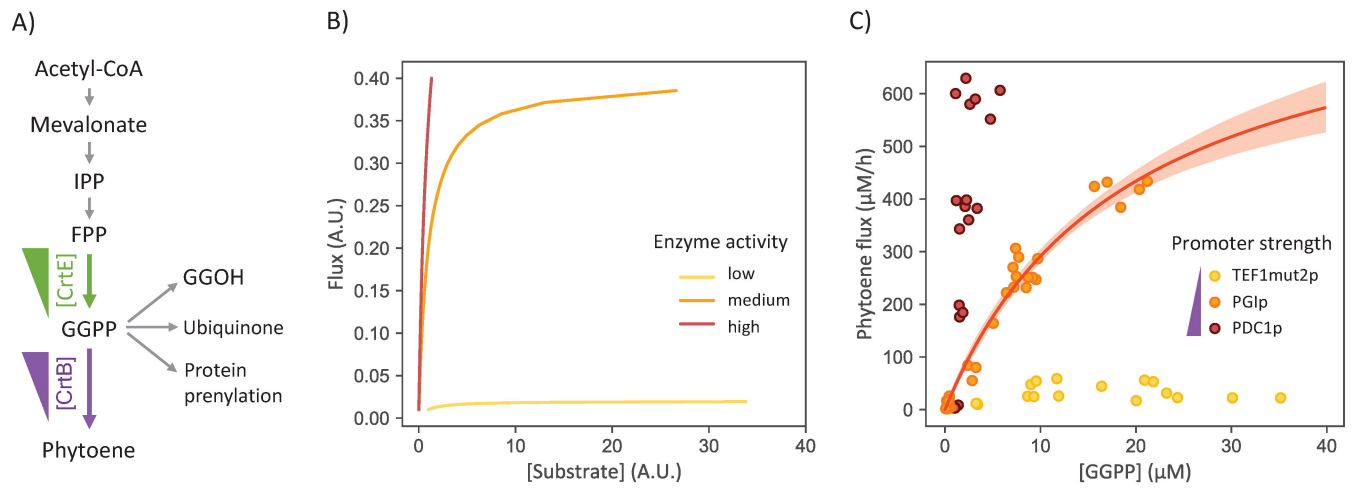
A)
Acetyl-CoA
Mevalonate
IPP
FPP
[CrtE]
GGPP
GGOH
Ubiquinone
Protein prenylation
[CrtB]
Phytoene
B)
Flux (A.U.)
[Substrate] (A.U.)
Enzyme activity
low
medium
high
C)
Phytoene flux (µM/h)
[GGPP] (µM)
Promoter strength
TEF1mut2p
PGIp
PDC1p

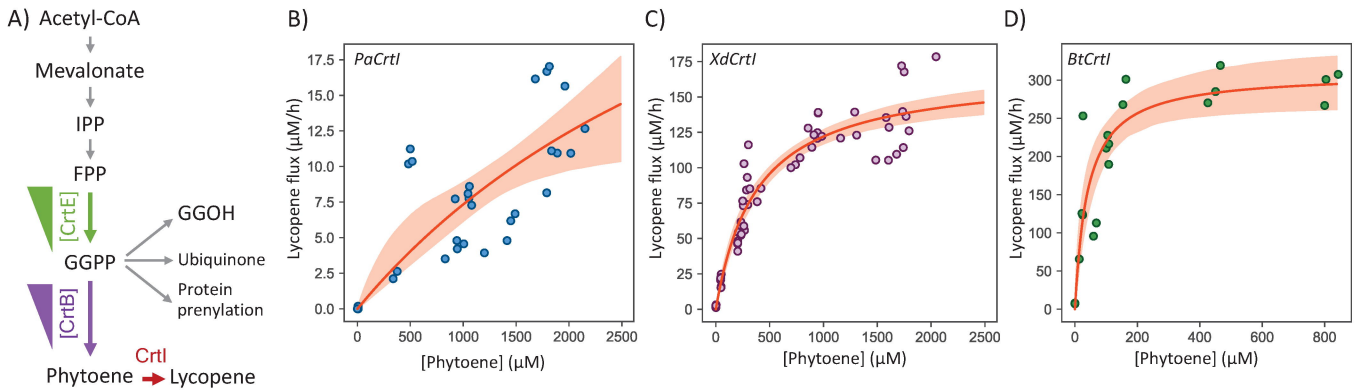
A)
Acetyl-CoA
Mevalonate
IPP
FPP
[CrtE]
GGPP
GGOH
Ubiquinone
Protein prenylation
[CrtB]
CrtI
Phytoene
Lycopene
B)
PaCrtI
Lycopene flux (μM/h)
[Phytoene] (μM)
C)
XdCrtI
Lycopene flux (μM/h)
[Phytoene] (μM)
D)
BtCrtI
Lycopene flux (μM/h)
[Phytoene] (μM)